Supplementary Materials:

Figures S1- S6, Legends and Figures

Table S1, S2

Online Methods

Supplementary References

Supplementary Fig. S1. Deletions of *siz1* or *siz2* partially reduce DSB relocation

(a) Cleavage efficiency in wild-type (GA6844), *siz1*Δ (GA-7899) and *siz2*Δ (GA-6858) strains determined by qPCR across the cleavage site. **(b)** Position of cleaved *MAT* in wild-type (GA-6844), *siz1*Δ (GA-7899) and *siz2*Δ (GA-6858) is shown following DSB induction (+ galactose) at indicated times. Assay was performed as described in Figure 1a-c. 33% (red dotted line) indicates random distribution.

Supplementary Fig. S2. Deletions of *slx5* or *slx8* reduce DSB recruitment to pores

(a) ChIP with the anti-pore monoclonal antibody, Mab414, monitors *MAT*α locus association with nuclear pores at the indicated time after addition of glucose (no cleavage) or galactose (HO cleavage) in wild-type (GA-3862), *slx5*Δ (GA-4105), *slx8*Δ (GA-4106) and wild-type no GAL-HO (*MAT**a***, GA-1080) cells. We cannot exclude that the *slx5*Δ culture was not partially diploidized in this assay, which might explain its two-fold higher level of pore recovery *vs.slx8*Δ. ChIP was carried out and results were processed as described in Nagai et al. (2008). **(b)** ChIP for HA-tagged Slx8 monitors *MAT* locus association with Slx8 at 1 h after cut induction on galactose in non-tagged (GA-3862) and Slx8-3HA (GA-3867) tagged cells. Distances of primers used for qPCR from the HO cut site are indicated and a probe 0.5kb from the end of telomere 6R is used as a control. ChIP was performed as in panel a.

Supplementary Fig. S3 Esc2 promotes DSB relocation to the nuclear pore in G1-phase cells, but is not sufficient for relocation a LexA-Esc2 targeting assay

(a) LexA-Slx8 complements the HU sensitivity observed in *slx8*Δ. Five-fold serial dilutions starting from $7x10^7$ cells for each indicated strain were spotted on SD-LEU medium containing indicated dose of HU and incubated at 30˚C for 4 days. Two independent clones were tested per strain. **(b)** *MAT* position relative to CFP-Nup49 in wild-type (GA-6844), and *esc2*Δ (GA-9373) after 120 min on galactose, as described in Figure 1a-c. # , significantly non-random distribution based on cell number and confidence values from a proportional test

between random and experimental distribution. * , significantly different distribution between wild-type and mutant. n.s., difference is not significant from random (33%), indicated by the red dotted line. **(c)** The position of *lacO*/LexA-tagged *PES4* was visualized by GFP-LacI and scored in the presence of LexA alone or a LexA-Esc2 fusion. Cells are classified into G1 or S phase. Strains carry GFP-Nup49 (GA-1461) and LexA fusion proteins are expressed from plasmids. Neither LexA nor LexA-Esc2 shift the tagged locus to the NE. n= cells counted; *P*=significance relative to a random distribution.

Supplementary Fig. S4. Localization of Slx5-GFP before or after γ-irradiation
(a,b) Slx5-GFP (green) and CFP-Nup49 (red) lare visualized by confocal microscopy in a wild-type strain (GA-8565). Cells are grown at 30°C in selective SC-L+G418 media and exposed to γ-irradiation (30 Gy). Prior to microscopy cells recovered during 2 h in SC-L+G418 media. Representative images (b) showing both peripheral (white arrows) and some internal Slx5 foci, particularly under conditions of irradiation, which induces nicks and oxidative damage, as well as DSBs. Spontaneous foci are of weaker intensity. Bars = 2μm

Supplementary Fig. S5. Slx5 binds Nse5, but not nse5-L247A, of the SMC5/6 complex
(a) Left panel compares the dimeric *S. cerevisiae* STUbL Slx5/Slx8, with its human homologue RNF4. The combination of SIM (SUMO-interacting motifs) and RING finger ubiquitin ligase function is characteristic of this class of enzyme. Right panel shows a sketch of the SMC5/6 complex with subunit names from budding yeast. **(b)** Analysis of Nse5 and wild-type Slx5 or $Slx5^{\Delta SIM}$ (in which SIMs at aa25-27 and aa93-96 are mutated) protein interactions by galactose-inducible yeast two-hybrid assays. Quantitative β-galactosidase assay is described in online Methods. Actual mean values of β-galactosidase activity are indicated beside bars. Interaction of Nse5 with Slx5 is monitored in *smt3-3KR* and the *smt3-331* loss-of-function mutant backgrounds. **(c)** Sketch of the Nse5 subunit. Nse5 has no recognizable SIM, although the L247 mutation interferes with both Slx5 and Smt3 interaction. Interaction of a fusion of Slx5-AD, Nse6-AD or of Smt3-AD with the wild-type Nse5 or $Nse5^{L247A}$, as bait are monitored as in (b).

Supplementary Fig. S6. The protein expression from yeast two-hybrid constructs
Plasmids J038 (Nse5-LexA) and J150 (Slx5-AD) which are both galactose inducible, were co-transformed into strains JC470 (wild-type), JC2996 (*smt3*-3KR), or JC2758 (*smt3*-331). Cells were treated with glucose (-) or galactose (+) at 30°C for 6 h and protein extracts were TCA precipitated prior to denaturation for 8% SDS-PAGE. Western blots were probed with

either anti-HA (Slx5-AD) or anti-LexA (Nse5-LexA; antibodies from Santa Cruz Biotechnology). Equal loading was confirmed by probing with anti-actin (Sigma). The *smt3*-331 mutation reduces but does not eliminate all SUMOylation.

Table S1. Summary of localization assay statistics

Figure	Experiment	Relevant genotype	min after HO	% of intact *MAT*	Cell cycle	# of nuclei	*P*-value (vs random/ wild-type)
Fig 1c, 2b, 5a, S3b	*MAT* zoning	Wild-type	120	4.27 ± 0.58	G1	169	**1.1×10^{-4}**
Fig 1c, 2b, 5a, S3b	*MAT* zoning	Wild-type	120	4.27 ± 0.58	S	108	**3.6×10^{-8}**
Fig 1c	*MAT* zoning	*siz1*Δ *siz2*Δ	120	6.51 ± 0.05	G1	321	0.24 / **1.8×10^{-4}**
Fig 1c	*MAT* zoning	*siz1*Δ *siz2*Δ	120	6.51 ± 0.05	S	64	0.48 / **8.3×10^{-3}**
Fig 1c	*MAT* zoning	*mms21*Δ*C*	120	6.08 ± 0.28	G1	146	9.0×10^{-2} / **1.7×10^{-4}**
Fig 1c	*MAT* zoning	*mms21*Δ*C*	120	6.08 ± 0.28	S	146	0.56 / **3.2×10^{-4}**
Fig 1d, 2c	Pore coloc.	Wild-type	0	100	G1	301	-
Fig 1d, 2c	Pore coloc.	Wild-type	40	10.60 ± 5.30	G1	299	-
Fig 1d, 2c	Pore coloc.	Wild-type	120	3.78 ± 1.08	G1	149	-
Fig 1d, 2c	Pore coloc.	Wild-type	0	100	S	94	-
Fig 1d, 2c	Pore coloc.	Wild-type	40	10.60 ± 5.30	S	88	-
Fig 1d	Pore coloc.	*siz2*Δ	0	100	G1	206	-
Fig 1d	Pore coloc.	*siz2*Δ	40	47.47 ± 0.66	G1	150	-
Fig 1d	Pore coloc.	*siz2*Δ	120	7.95 ± 0.82	G1	129	-
Fig 1d	Pore coloc.	*siz2*Δ	0	100	S	62	-
Fig 1d	Pore coloc.	*siz2*Δ	40	47.47 ± 0.66	S	51	-
Fig 1g	*MAT* zoning	*smt3-3KR*	120	6.21 ± 0.37	G1	279	0.20
Fig 1g	*MAT* zoning	*smt3-3KR*	120	6.21 ± 0.37	S	71	0.36
Fig 2b	*MAT* zoning	*slx5*Δ	120	4.34 ± 0.98	G1	110	0.89 / **1.6×10^{-2}**
Fig 2b	*MAT* zoning	*slx5*Δ	120	4.34 ± 0.98	S	63	**1.6×10^{-2}** / 0.17
Fig 2b	*MAT* zoning	*slx8*Δ	120	6.83 ± 1.06	G1	108	0.68 / **4.6×10^{-2}**

Fig 2b	*MAT* zoning	*slx8*Δ	120	6.83 ± 1.06	S	68	**3.2×10^{-2}** / $\underline{9.9\times10^{-2}}$
Fig 2c	Pore coloc.	*slx5*Δ	0	100	G1	202	-
Fig 2c	Pore coloc.	*slx5*Δ	40	13.11 ± 1.49	G1	152	-
Fig 2c	Pore coloc.	*slx5*Δ	120	9.32 ± 0.81	G1	133	-
Fig 2c	Pore coloc.	*slx5*Δ	0	100	S	50	-
Fig 2c	Pore coloc.	*slx5*Δ	40	13.11 ± 1.49	S	34	-
Fig 3b, 4a, S3c	Targeting, zoning	LexA/WT	-	-	G1	147	0.73
Fig 3b, 4a, S3c	Targeting, zoning	LexA/WT	-	-	S	105	0.68
Fig 3b	Targeting, zoning	LexA-polySmt3/WT	-	-	G1	116	**$< 1.0\times10^{-30}$**
Fig 3b	Targeting, zoning	LexA-polySmt3/WT	-	-	S	82	0.18
Fig 3b	Targeting, zoning	LexA-polySmt3/*siz2*Δ	-	-	G1	139	**$4.0\text{x}10^{-4}$**
Fig 3b	Targeting, zoning	LexA-polySmt3/*siz2*Δ	-	-	S	92	0.30
Fig 3b	Targeting, zoning	LexA-polySmt3/*slx5*Δ	-	-	G1	88	0.88
Fig 3b	Targeting, zoning	LexA-polySmt3/*slx5*Δ	-	-	S	198	0.55
Fig 3c	Targeting, zoning	LexA-Slx5/WT	-	-	G1	102	**6.6×10^{-5}**
Fig 3c	Targeting, zoning	LexA-Slx5/WT	-	-	S	84	0.49
Fig 3c	Targeting, zoning	LexA-Slx5/*siz2*Δ	-	-	G1	178	**1.4×10^{-8}**
Fig 3c	Targeting, zoning	LexA-Slx5/*siz2*Δ	-	-	S	75	0.62
Fig 3c	Targeting, zoning	LexA-Slx5/*slx8*Δ	-	-	G1	80	**3.9×10^{-5}**
Fig 3c	Targeting, zoning	LexA-Slx5/*slx8*Δ	-	-	S	95	7.0×10^{-2}
Fig 3c	Targeting, zoning	LexA-Slx8/WT	-	-	G1	138	0.28
Fig 3c	Targeting, zoning	LexA-Slx8/WT	-	-	S	70	0.27
Fig 3d, 4b	Targeting, pore coloc.	LexA	-	-	G1	129	-
Fig 3d, 4b	Targeting,	LexA	-	-	S	101	-

	pore coloc.						
Fig 3d	Targeting, pore coloc.	LexA-polySmt3	-	-	G1	179	-
Fig 3d	Targeting, pore coloc.	LexA-polySmt3	-	-	S	106	-
Fig 3d	Targeting, pore coloc.	LexA-Slx5	-	-	G1	131	-
Fig 3d	Targeting, pore coloc.	LexA-Slx5	-	-	S	104	-
Fig 4a	Targeting, zoning	LexA-Smt3/WT	-	-	G1	110	0.20
Fig 4a	Targeting, zoning	LexA-Smt3/WT	-	-	S	105	**5.3×10^{-6}**
Fig 4a	Targeting, zoning	LexA-smt3-3KR/WT	-	-	G1	84	0.35
Fig 4a	Targeting, zoning	LexA-smt3-3KR/WT	-	-	S	93	**2.1×10^{-3}**
Fig 4a	Targeting, zoning	LexA-smt3-3KR/*siz2*Δ	-	-	G1	116	0.39
Fig 4a	Targeting, zoning	LexA-smt3-3KR/*siz2*Δ	-	-	S	105	**$3.8\text{x}10^{-3}$**
Fig 4b	Targeting, pore coloc.	LexA-Smt3	-	-	G1	131	-
Fig 4b	Targeting, pore coloc.	LexA-Smt3	-	-	S	104	-
Fig 4b	Targeting, pore coloc.	LexA-smt3-3KR	-	-	G1	145	-
Fig 4b	Targeting, pore coloc.	LexA-smt3-3KR	-	-	S	112	-
Fig 4c	Targeting, zoning	LexA-smt3-3KR and control vector	-	-	G1	95	0.25
Fig 4c	Targeting, zoning	LexA-smt3-3KR and control vector	-	-	S	83	**2.0×10^{-5}**
Fig 4c	Targeting, zoning	LexA-smt3-3KR and Mps3N’	-	-	G1	93	0.51
Fig 4c	Targeting, zoning	LexA-smt3-3KR and Mps3N’	-	-	S	143	0.34
Fig 5b	*MAT* zoning	*nse5-L247A*	120	8.24 ± 0.23	G1	194	**2.0×10^{-3}** / 0.50
Fig 5b	*MAT* zoning	*nse5-L247A*	120	8.24 ± 0.23	S	95	0.35 / **3.7×10^{-3}**
Fig 5b	*MAT* zoning	*smc6-9*	120	14.45 ± 1.19	G1	191	0.96 / **7.5×10^{-3}**

Fig 5b	*MAT* zoning	*smc6-9*	120	14.45 ± 1.19	S	61	0.86 / **2.8×10^{-3}**
Fig 5b	*MAT* zoning	*rtt107*Δ	120	5.01 ± 0.45	G1	252	0.32
Fig 5b	*MAT* zoning	*rtt107*Δ	120	5.01 ± 0.45	S	106	0.28
Fig S1a, b	*MAT* zoning	Wild-type	0	100	G1/S/G2	198	1
Fig S1a, b	*MAT* zoning	Wild-type	20	20.43 ± 5.19	G1/S/G2	206	**4.3×10^{-3}**
Fig S1a, b	*MAT* zoning	Wild-type	40	15.95 ± 9.68	G1/S/G2	225	**2.0×10^{-10}**
Fig S1a, b	*MAT* zoning	Wild-type	60	6.60 ± 0.33	G1/S/G2	218	**< 1.0×10^{-30}**
Fig S1a, b	*MAT* zoning	Wild-type	120	4.79 ± 2.14	G1/S/G2	211	**5.3×10^{-5}**
Fig S1a, b	*MAT* zoning	*siz1*Δ	0	100	G1/S/G2	267	0.19
Fig S1a, b	*MAT* zoning	*siz1*Δ	20	34.64 ± 6.92	G1/S/G2	233	0.75
Fig S1a, b	*MAT* zoning	*siz1*Δ	40	11.54 ± 0.79	G1/S/G2	185	**1.1×10^{-2}**
Fig S1a, b	*MAT* zoning	*siz1*Δ	60	8.06 ± 0.07	G1/S/G2	282	**3.0×10^{-6}**
Fig S1a, b	*MAT* zoning	*siz1*Δ	120	8.04 ± 0.79	G1/S/G2	191	0.26
Fig S1a, b	*MAT* zoning	*siz2*Δ	0	100	G1/S/G2	135	0.27
Fig S1a, b	*MAT* zoning	*siz2*Δ	20	40.89 ± 2.13	G1/S/G2	101	0.78
Fig S1a, b	*MAT* zoning	*siz2*Δ	40	20.37 ± 3.36	G1/S/G2	111	**4.4×10^{-2}**
Fig S1a, b	*MAT* zoning	*siz2*Δ	60	15.39 ± 1.23	G1/S/G2	124	**2.6×10^{-2}**
Fig S1a, b	*MAT* zoning	*siz2*Δ	120	9.93 ± 1.77	G1/S/G2	125	**6.5×10^{-3}**
Fig S3b	*MAT* zoning	*esc2*Δ	120	14.95 ± 4.19	G1	179	0.49 / **$\underline{5.1\times10^{-4}}$**
Fig S3b	*MAT* zoning	*esc2*Δ	120	14.95 ± 4.19	S	96	**9.7×10^{-5}** / $\underline{0.97}$
Fig S3c	Targeting, zoning	LexA-Esc2/WT	-	-	G1	104	0.78
Fig S3c	Targeting, zoning	LexA-Esc2/WT	-	-	S	130	0.42

Bold face: significantly non-random

Table S2. Yeast strains used in this study

Name	Genotype	Source
GA-1081	JKM179; *MAT*α, Δ*ho hml::ADE1 hmr::ADE1 ade3::GALHO ade1-100 leu2-3, 112 lys5 trp1::hisG ura3-52*	(Lee et al. 1998)
GA-6844	GA-1081 *CFP-NUP49 GFP-LacI:Leu2 MAT::LacO* repeats*:TRP1*	(Horigome et al. 2014)
GA-7968	GA-6844 *siz1::natMX4 siz2::C.a.URA3*	This study
JC3654	GA-6844 *mms21ΔC:HYG*	This study
GA-7314	GA-6844 *nup133::natMX4* pUN100-*nup133ΔN:kanMX6*	This study
GA-7970	GA-7314 *siz2::C.a.URA3*	This study
GA-6858	GA-6844 *siz2::KanMX*	This study
GA-1259	JKM139; *MAT***a**, Δ*ho hml::ADE1 hmr::ADE1 ade3::GALHO ade1-100 leu2-3, 112 lys5 trp1::hisG ura3-52*	(Lee et al. 1998)
GA-8306	GA-1259 *3HA-MPS3*	(Lee et al. 1998; Horigome et al. 2014)
GA-8541	GA-8306 *siz2::natMX4*	This study
GA-9072 (JC3656)	GA-6844 *smt3-3KR:HYG*	This study
GA-1081 (JC727)	JKM179; *MAT*α, Δ*ho hml::ADE1 hmr::ADE1 ade3::GALHO ade1-100 leu2-3, 112 lys5 trp1::hisG ura3-52*	(Lee et al. 1998)
JC3020	JC727 *SLX5-3HA::URA3*	This study
JC3668	JC3020 *siz2::KanMX6*	This study
JC3214	JC3020 *smt3-K11R,K15R,K19R::TRP1*	This study
GA-7097	GA-6844 *slx5::natMX4*	This study
GA-7098	GA-6844 *slx8::natMX4*	This study
GA-7969	GA-7314 *slx5::C.a.URA3*	This study
GA-8539	GA-8306 *slx5::natMX4*	This study
GA-8194	W303 *MAT***a**, *ade2-1 trp1-1 his3-11 his3-15 ura3-1 leu2-3 leu1-112 can1-100 nup133::HIS3* -pUN100-*nup133ΔN:kanMX6 CFP-NUP49 ade2::lacI-GFP:ADE2 lys2::LexALacOPs:TRP*	This study
GA-1461	W303 *MAT***a**, *PES4:4xLexA:lacO array:TRP1 his3-15::GFP-LacI:HIS3 NUP49-GFP*	(Heun et al. 2001)
GA-4447	GA-1461 *siz2::KanMX6*	This study
GA-4448	GA-1461 *slx5::KanMX6*	This study
GA-4449	GA-1461 *slx8::KanMX6*	This study
JC3161	GA-6844 *nse5::HYG ura3:: nse5-L247A:URA3*	This study
JC3131	GA-6844 *smc6-9::KanMX4*	This study

GA-7092	GA-6844 *rtt107::natMX4*	This study
GA-4133	GA-1081 *NUP84-13MYC*	This study
JC3154	GA-4133 *nse5::HYG ura3:: nse5-L247A:URA3*	This study
JC3150	GA-4133 *smc6-9::KanMX4*	This study
JC3167	GA-1081 *3HA-MPS3:URA3*	This study
JC3114	JC3167 *nse5::HYG ura3:: nse5-L247A:URA3*	This study
JC3115	JC3167 *smc6-9::KanMX4*	This study
JC3621	JC3020 *nse5::HYG ura3:: nse5-L247A:URA3*	This study
JC3189	JC3020 *smc6-9::KanMX*	This study
GA-9206	GA-6844 *siz2::HPH slx5::natMX4*	This study
GA-9355	GA-6844 *nse5-L247A:URA3 slx5::HYG*	This study
GA-8994	W303 *MATa-inc, lys2::NatMX4 AVT2::ly-HOcs::KanMX6 ERV46::TRP1-ys2 (Ch I 60kb donor) ade3::GAL-HO URA3::TK BAR1::LEU2*	(Donnianni and Symington 2013)
GA-9185	GA-8994 *nup60::hphMX4*	This study
GA-9186	GA-8994 *slx8::hphMX4*	This study
GA-9090	GA-8994 *pol32::hphMX4*	This study
GA-8860	GA-1081 *CFP-NUP49 GFP-LacI:Leu2 MAT::LacO* repeats*:TRP1*	This study
GA-8471	GA-6844 *nup84::natMX4*	This study
GA-7899	GA-6844 *siz1::natMX4*	This study
GA-3862	JKM139; *MAT***a**, Δ*ho hml::ADE1 hmr::ADE1 ade3::GALHO ade1-100 leu2-3, 112 lys5 trp1::hisG ura3-52*	Gift from Nevan Krogan
GA-4105	GA-3862 *slx5::caURA3*	This study
GA-4106	GA-3862 *slx8::caURA3*	This study
GA-1080	JKM115; *MAT*α, Δ*ho hml::ADE1 hmr::ADE1 ade1-100 leu2-3, 112 lys5 trp1::hisG ura3-52*	Gift from James E. Haber
GA-3867	KLY3; GA-3862 *slx5::Slx5-3HA:KL-TRP*	Gift from Michael Keogh
GA-9373	GA-6844 *esc2::natMX4*	This study
GA-7451	YOK851; *MAT*α, *his3-*Δ*200 leu2-3, 112 ura3-52 lys2-80 trp1-1 gal2 slx5::kanMX4 SLX5-GFP:LEU2/CEN*	(Cook et al. 2009)
GA-8565	GA-7451 *CFP-NUP49*	This study
JC470	W303 *MAT***a**, *ade2-1 trp1-1 his3-11 his3-15 ura3-1 leu2-3 leu2-112, RAD5+*	This study
JC2758	JC470 *smt3-331*	This study
JC2996	JC470 *smt3K11R, K15R, K19R::TRP1* (*smt3-3KR*)	This study

Online Methods

Plasmids, yeast strains and yeast techniques

Yeast strains used in this study are described in Table S2. JKM139 and JKM179 are gifts from J. E. Haber and have been previously described (Lee et al. 1998). Standard methods for genetic modification of yeast were used (Longtine et al. 1998) and were verified by PCR and phenotypic analysis. Yeast strains with *3HA-MPS3* were created by using the plasmid pRS306-*3HA-MPS3* (gift from Dr. Mizuta) (Horigome et al. 2011). For DSB localization a *lacO* array initially containing 256 lacI binding sites was inserted at 4.4 kb from the HO cut site at *MAT* (Nagai et al. 2008). Note that repeat number is not stable in all strains and is usually less than 256. For DSB localization, cells were grown at 30°C for 2 days on YPAD plate (or selective SC media if required), then inoculated into synthetic media containing 0.05% glucose, 3% glycerol and 2% lactate (SCLGg) and grown overnight to obtain an exponentially growing cell population with no more than 5-7×10^6 cells ml^{-1}. Galactose (20%) is added to final 2% to induce the HO endonuclease. Cells were harvested, fixed with para-formaldehyde (final 4%) and washed 3 times with PBS at indicated time points. Cell cycle stages were assigned as follows: G1 cells have no bud and a round nucleus, cells in S phase have a bud up to 2/3 the size of the mother cells and a round nucleus. G2 cells have nuclei at the bud neck; such nuclei are usually distorted and therefore not reliable for position analysis.

Targeting constructs and strains

Like the LexA-Slx5, -Slx8 and -Esc2 fusion, LexA fusions to 4xSmt3 to a single Smt3 or smt3-3KR moiety were created in and expressed from the plasmid pAT4. The 4xSmt3 construct (LexA-polySUMO) was created by cloning four Smt3 genes tandemly into the vector pAT4 using a 4xSmt3 construct synthesized by Bio Basic Inc. Gene Synthesis. To prevent processing of the internal SUMO proteins by Ulp1, the constructs were truncated at I_{96} to remove the di-glycine motif. The fourth SUMO residue in the chain retains the full SUMO sequence including the di-glycine motif. The single Smt3 moiety is not mutated and can be a substrate for polySUMOylation while smt3-3KR cannot. Targeted binding of LexA fusions to the indicated loci is described in (Neumann et al. 2012; Horigome et al. 2014).

Microscopy and image analysis

Fluorescence microscopy and quantification was performed according to published methods (Meister et al. 2010; Horigome et al. 2015). Images for zoning measurements were captured

on a Metamorph-driven Spinning-disk confocal system based on an Olympus IX81 microscope, Yokogawa CSU-X1 scan head, EM-CCD Cascade II (Photometrics) camera and an ASI MS-2000 Z-piezo stage. We used PlanApo ×100, NA 1.45 total internal reflection fluorescence microscope oil objective. LacI-GFP position was determined with a through-focus stack of 16-21 0.2 μm steps and was measured by ImageJ (NIH, USA) and the plug-in software PointPicker (Meister et al. 2010). The numbers of nuclei scored are in Table S1.

Statistical analyses and cutting efficiency

To determine zone enrichment we applied a $\chi 2$ test comparing zone1 to a random distribution (degree of freedom = 2, confidence limit = 95%). *P*-values are listed in Table S1. To compare the perinuclear enrichment of two different strains, we used a proportional analysis with a confidence limit of 95%. The error bars of all ChIP experiments represent the s.e.m.

The efficiency of DSB induction was determined by qPCR using TaqMan probes as described (van Attikum et al. 2007). The value was normalized to cut efficiency and PCR efficiency at an uncut locus, *SMC2*. Primer and probe sequences are available on request. The cutting efficiencies are available in Table S1.

Chromatin immunoprecipitation (ChIP) assays

ChIP with anti-HA or anti-MYC epitope tagged strains was carried out as previously described (Yoshida et al. 2010) with the following modifications. Yeast cells cultured in 45 ml medium were cross-linked at 30°C for 20 min, and disrupted using a bead beater (TOMY) and Zirconia/Silica beads. The recovered chromatin fraction was subjected to sonication using Bioruptor Plus (Diagenode) to obtain fragmented chromatin < 500 bp in length. An anti-HA antibody (sc-7392, Santa Cruz Biotech, Inc), an anti-MYC antibody (9E10) combined with anti-mouse IgG magnetic beads (Invitrogen) or Protein G magnetic beads (Invitrogen), respectively, were used for IP. ChIP DNA was purified and was analysed by quantitative PCR using primers adapted to the *MAT***a** or *MAT*α locus (available on request). ChIP with Mab414 (Abcam) was performed basically as described (H. Van Attikum et al. 2007) using the indicated strains. Input and IP DNA were purified and analyzed by real-time (rt) PCR, using the Perkin-Elmer ABI Prism 7700 Sequence Detector System. For each ChIP, rtPCR was performed two or three times. Absolute enrichment was calculated as follows: for each time point, the signal from a site near the HO DSB at *MAT* was normalized to that from either genomic *SMC2* locus or mitochondrial *OLI1* locus in ChIP and input DNA samples. For each time point and site, normalized ChIP signals were normalized to input DNA signals.

Repair assays

Precise and imprecise NHEJ were performed as described in (van Attikum et al. 2007), using isogenic derivatives of GA-1081 (i.e. GA-8860, wild-type and GA-8471, *nup84*Δ). For imprecise NHEJ, cells were grown in YPLGg to OD600 0.6-1.2. They were plated on 2% galactose plates, and scored for CFUs after 2-3 days at 30°C. For precise NHEJ, cells were grown in YPLGg to log phase, HO was induced with 2% galactose for 75 min, cells were washed 2x and shaken in YPD for 2 h. Samples for qPCR were taken before galactose addition (0 min), after gal addition (75 min) and after YPD recovery (195 min). Genomic DNA was extracted and used for real-time PCR (primers available upon request). Formulas for NHEJ efficiency are described in van Attikum et al., 2007.. Survival after HO-induced cleavage was performed by standard induction of HO-cleavage on galactose for up to 4 h, followed by washing of the cells and plating in triplicate on YPAD. CFU were scored after 2 days at 30°C.

The Break-induced replication (BIR) assay was performed, and the frequency of recombinants was calculated, as previously described (Donnianni and Symington 2013). Briefly, 4 individual colonies per strain were grown to exponential phase in YPR (1% yeast extract, 2% peptone, 2% raffinose), and then plated on YP containing 2% Glucose or 2% Galactose in 3 serial dilutions. CFU were counted after 3 days. Plates were replica plated on SC-Lys and YPD+G418 to determine the frequency of BIR recombinants, which is the ratio of colonies growing on SC-Lys over those growing on YPGalactose, divided by the plating efficiency.

Two-hybrid Analysis

NSE5 versions were cloned into pEG202-derived bait plasmids, creating Nse5-LexA fusion proteins, while *SLX5* genes were cloned into pJG4-6-derived prey plasmids creating Slx5-B42-activating domain fusion proteins. *nse5L247A* was generated by site-directed mutagenesis, while *slx5ΔSIM* was generated by subcloning *slx5SIMA/B* from the pAA3-derived plasmid published in (Cook et al. 2009). Bait and prey plasmids, as well as the reporter plasmid pSH18034, were transformed into W303 wild type strain JC470, JC2996 (*smt3-3KR*), or JC2758 (*smt3-331*). Protein-protein interactions were measured by quantitative β-galactosidase activity for permeabilized cells, and represent the averages of three independent experiments, with error bars indicating S.D.

References

Cook CE, Hochstrasser M, Kerscher O. 2009. The SUMO-targeted ubiquitin ligase subunit Slx5 resides in nuclear foci and at sites of DNA breaks. *Cell cycle (Georgetown, Tex)* **8**: 1080-1089.

Donnianni RA, Symington LS. 2013. Break-induced replication occurs by conservative DNA synthesis. *Proceedings of the National Academy of Sciences of the United States of America* **110**: 13475-13480.

Heun P, Laroche T, Shimada K, Furrer P, Gasser SM. 2001. Chromosome dynamics in the yeast interphase nucleus. *Science (New York, NY)* **294**: 2181-2186.

Horigome C, Dion V, Seeber A, Gehlen LR, Gasser SM. 2015. Visualizing the spatiotemporal dynamics of DNA damage in budding yeast. *Methods in molecular biology* **1292**: 77-96.

Horigome C, Okada T, Shimazu K, Gasser SM, Mizuta K. 2011. Ribosome biogenesis factors bind a nuclear envelope SUN domain protein to cluster yeast telomeres. *The EMBO journal* **30**: 3799-3811.

Horigome C, Oma Y, Konishi T, Schmid R, Marcomini I, Hauer MH, Dion V, Harata M, Gasser SM. 2014. SWR1 and INO80 chromatin remodelers contribute to DNA double-strand break perinuclear anchorage site choice. *Molecular cell* **55**: 626-639.

Lee SE, Moore JK, Holmes A, Umezu K, Kolodner RD, Haber JE. 1998. Saccharomyces Ku70, mre11/rad50 and RPA proteins regulate adaptation to G2/M arrest after DNA damage. *Cell* **94**: 399-409.

Longtine MS, McKenzie A, 3rd, Demarini DJ, Shah NG, Wach A, Brachat A, Philippsen P, Pringle JR. 1998. Additional modules for versatile and economical PCR-based gene deletion and modification in Saccharomyces cerevisiae. *Yeast (Chichester, England)* **14**: 953-961.

Meister P, Gehlen LR, Varela E, Kalck V, Gasser SM. 2010. Visualizing yeast chromosomes and nuclear architecture. *Methods in enzymology* **470**: 535-567.

Nagai S, Dubrana K, Tsai-Pflugfelder M, Davidson MB, Roberts TM, Brown GW, Varela E, Hediger F, Gasser SM, Krogan NJ. 2008. Functional targeting of DNA damage to a nuclear pore-associated SUMO-dependent ubiquitin ligase. *Science (New York, NY)* **322**: 597-602.

Neumann FR, Dion V, Gehlen LR, Tsai-Pflugfelder M, Schmid R, Taddei A, Gasser SM. 2012. Targeted INO80 enhances subnuclear chromatin movement and ectopic homologous recombination. *Genes & development* **26**: 369-383.

van Attikum H, Fritsch O, Gasser SM. 2007. Distinct roles for SWR1 and INO80 chromatin remodeling complexes at chromosomal double-strand breaks. *The EMBO journal* **26**: 4113-4125.

Yoshida T, Shimada K, Oma Y, Kalck V, Akimura K, Taddei A, Iwahashi H, Kugou K, Ohta K, Gasser SM et al. 2010. Actin-related protein Arp6 influences H2A.Z-dependent and -independent gene expression and links ribosomal protein genes to nuclear pores. *PLoS genetics* **6**: e1000910.

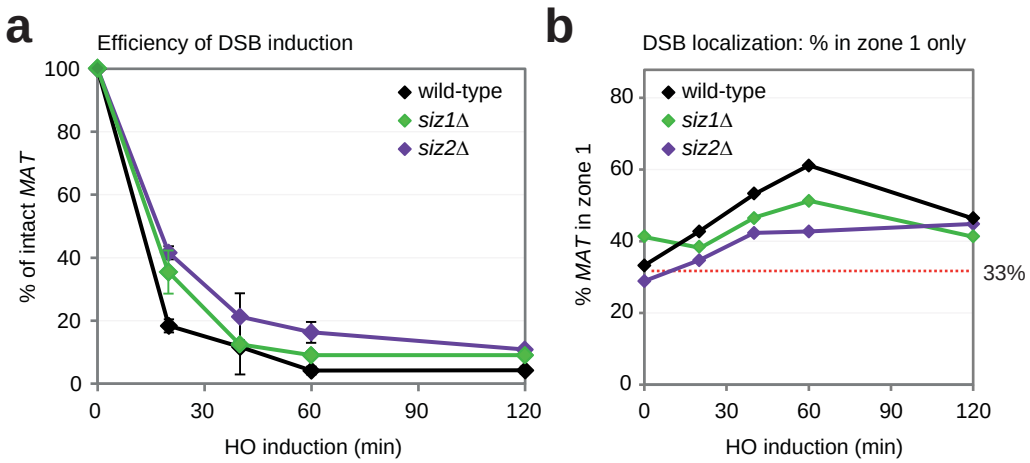

Horigome *et al.*, Figure S1

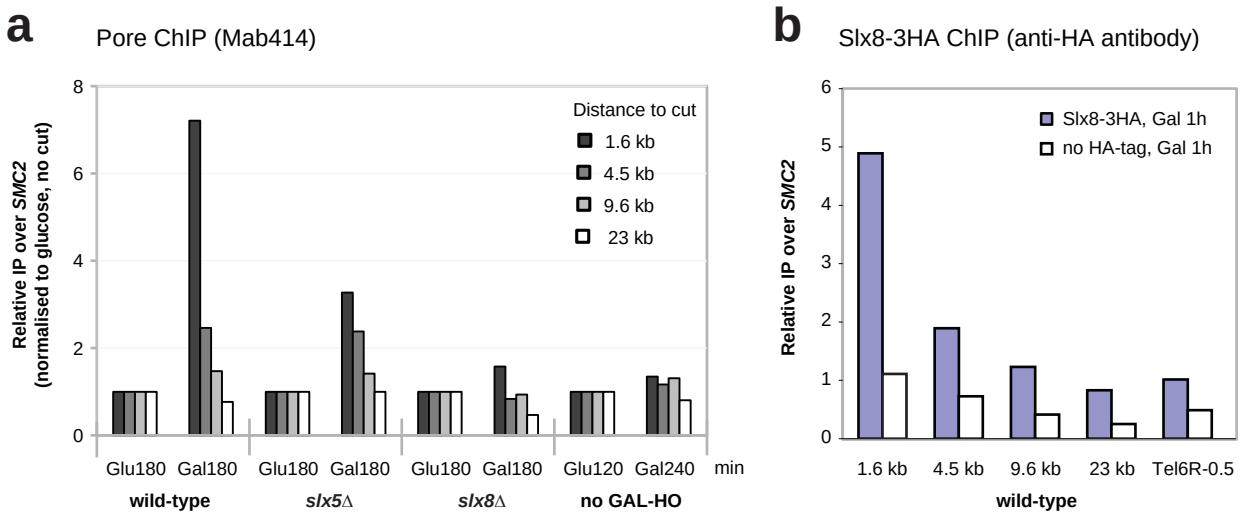

Horigome *et al.*, Figure S2

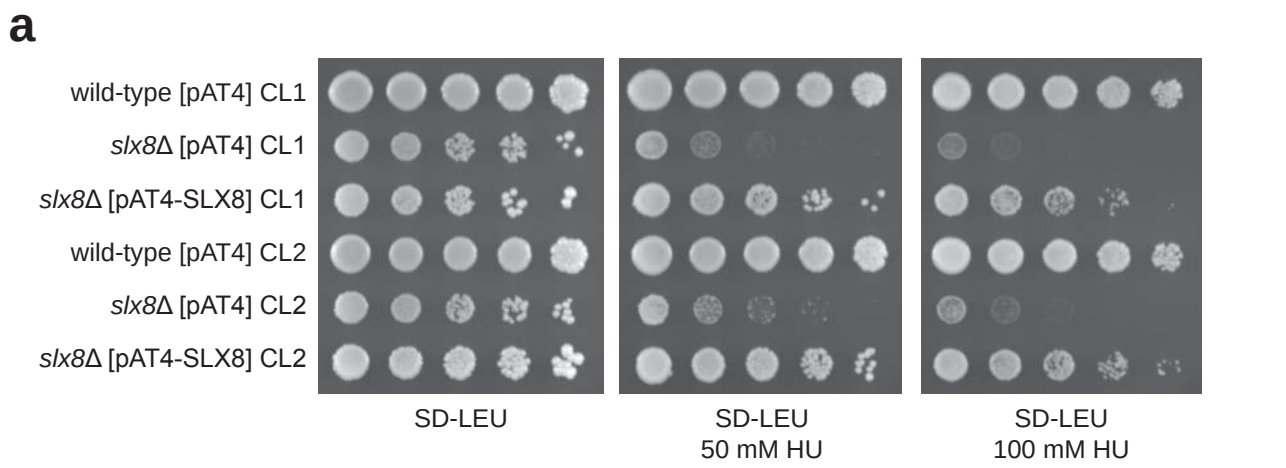

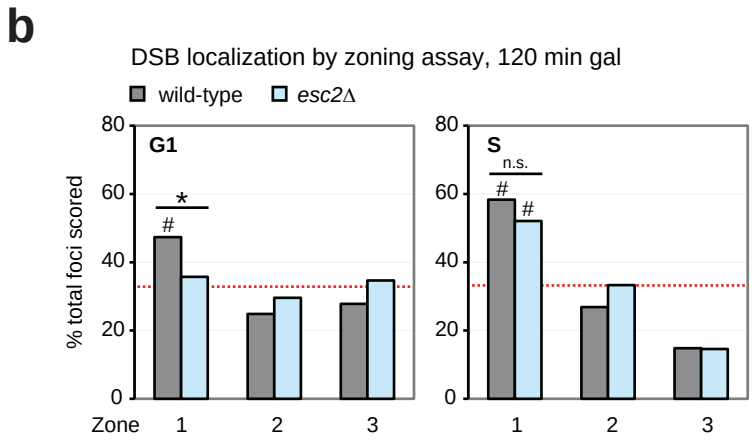

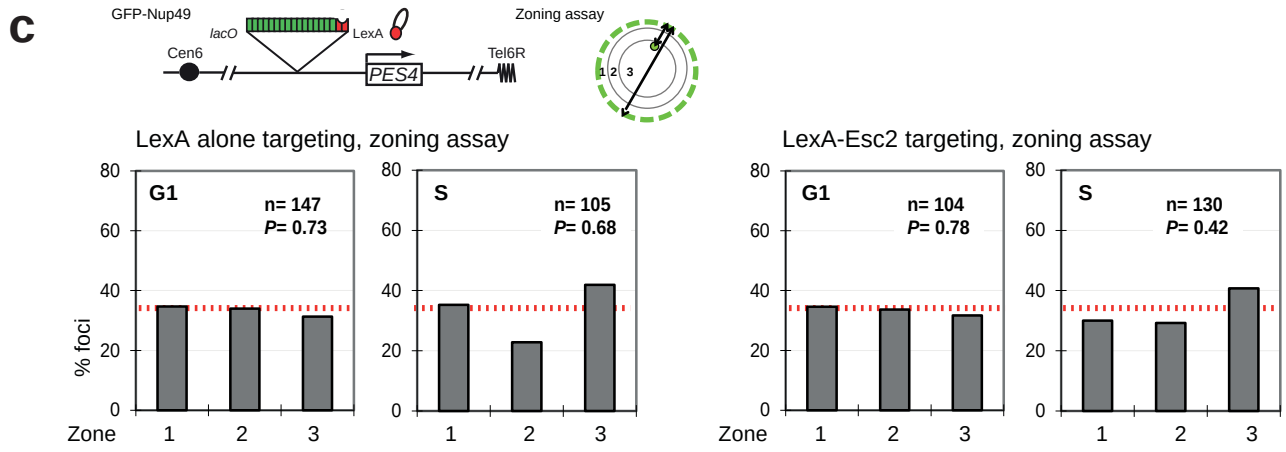

Horigome *et al.*, Figure S3

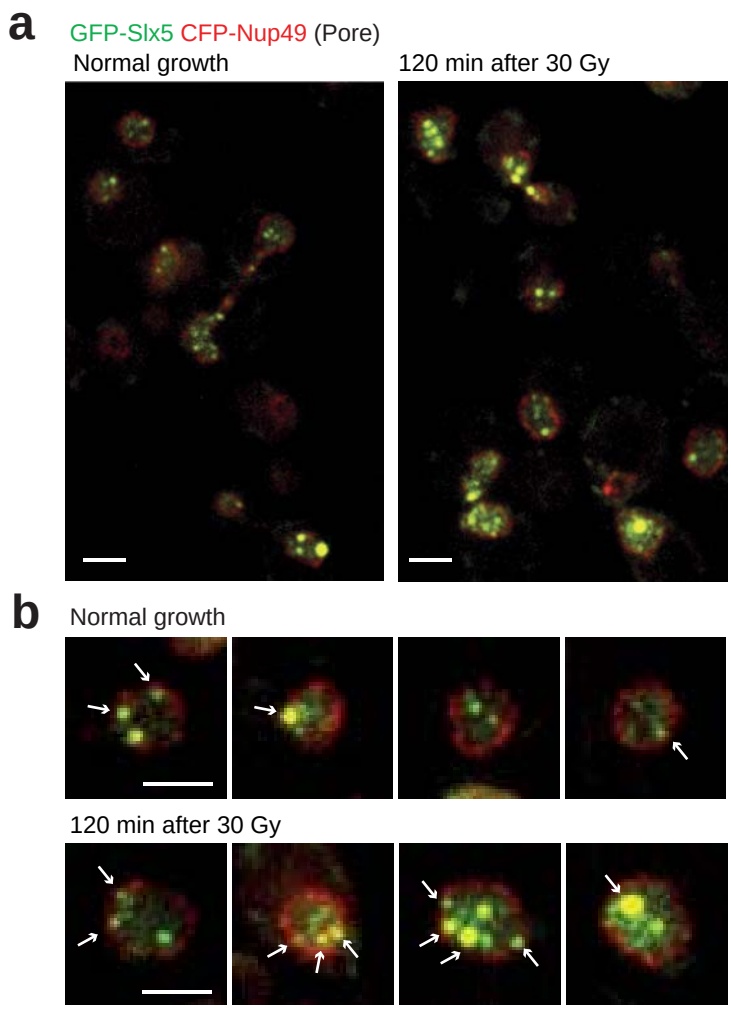

Horigome *et al.*, Figure S4

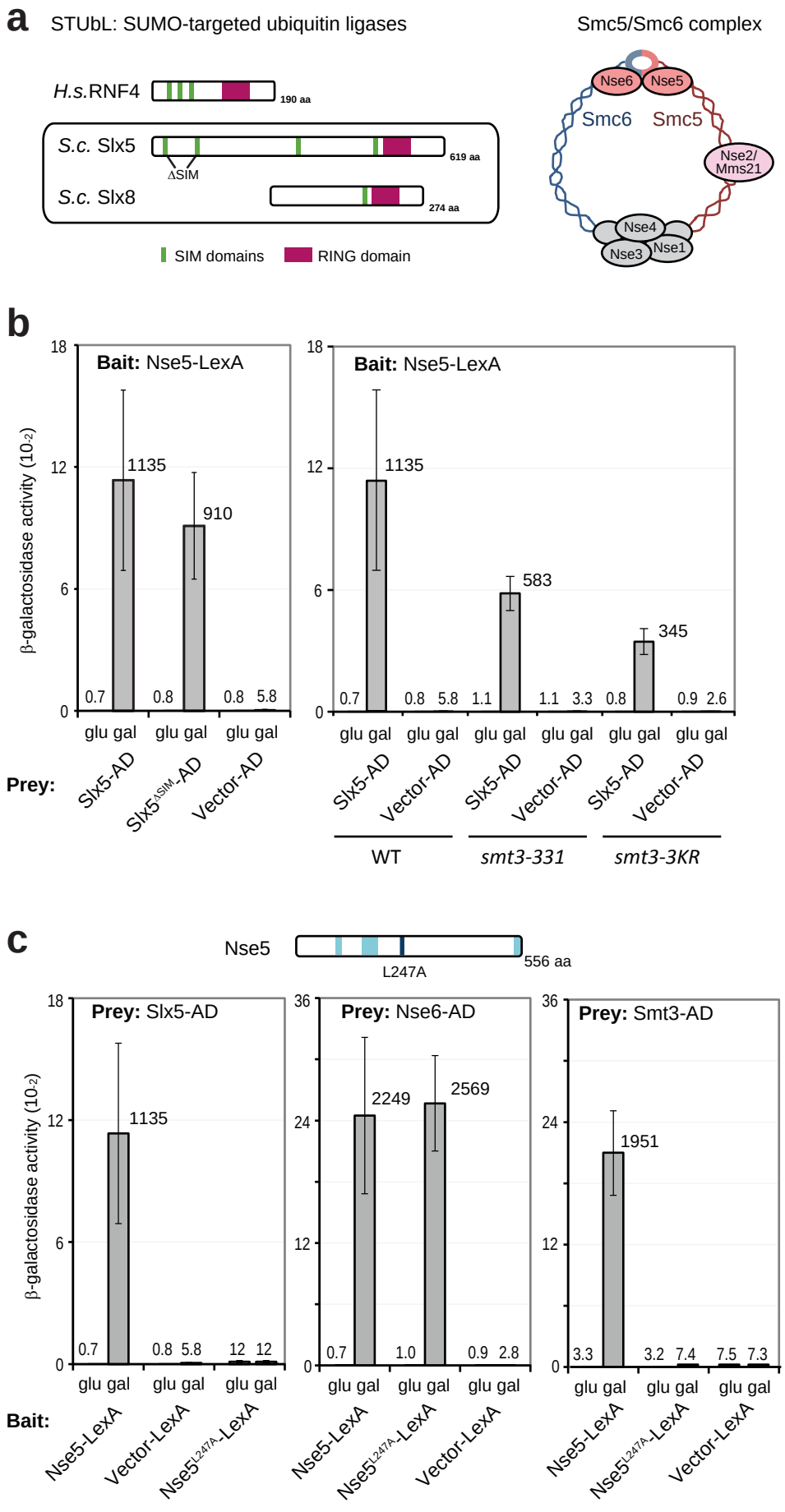

Horigome *et al.*, Figure S5

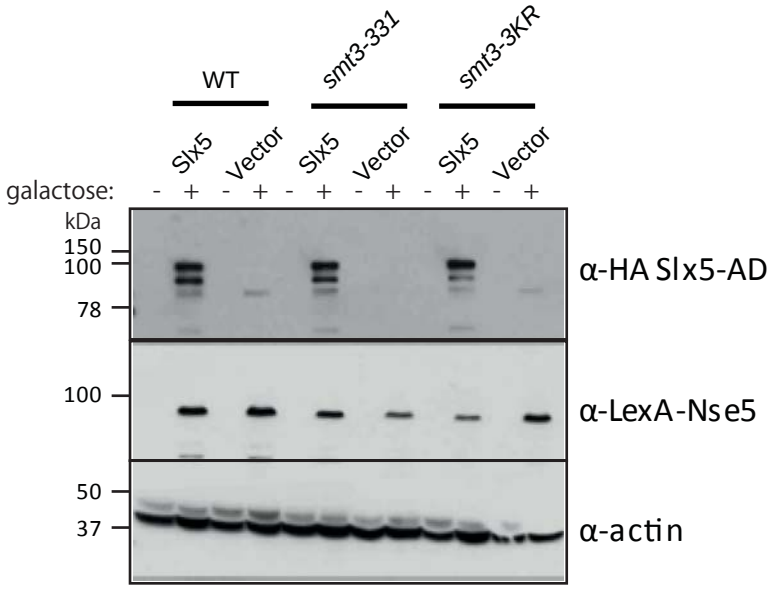

Horigome *et al.*, Figure S6